Rafael Serra-Gómez, Cécile A. Dreiss, Javier González-Benito, and Gustavo González-Gaitano
Langmuir 2016 32 (25), 6398-6408

DOI: 10.1021/acs.langmuir.6b01544

Structure and Rheology of Poloxamine T1107 and its Nanocomposite Hydrogels with Cyclodextrin-Modified Barium Titanate Nanoparticles

Rafael Serra-Gómez[a], *Cécile A. Dreiss**[c], *Javier González-Benito*[b], *Gustavo González-Gaitano**[a]

[a] Departamento de Química, Universidad de Navarra, 31080 Pamplona, Spain
[b] Department of Materials Science and Engineering, IQMAAB, Universidad Carlos III de Madrid, 28911 Leganés, Spain
[c] Institute of Pharmaceutical Science, King's College London, Franklin-Wilkins Building, 150 Stamford Street, London SE1 9NH, UK

Corresponding Authors: gaitano@unav.es, cecile.dreiss@kcl.ac.uk

Abstract

We report the preparation of a nanocomposite hydrogel based on a poloxamine gel matrix (Tetronic T1107) and cyclodextrin (CD)-modified Barium Titanate (BT) nanoparticles. The micellization and sol-gel behaviour of pH-responsive block-copolymer T1107 were fully characterised by small-angle neutron scattering (SANS), dynamic light scattering (DLS), and FTIR-ATR spectroscopy as a function of concentration, pH and temperature. SANS results reveal that spherical micelles in the low concentration regime present a dehydrated core and highly hydrated shell, with a small aggregation number and size, highly dependent on the degree of protonation of the central amine spacer. At high concentration, T1107 undergoes a sol-gel transition, which is inhibited at acidic pH. Nanocomposites were prepared by incorporating CD-modified BT of two different sizes (50 nm and 200 nm) in concentrated polymer solutions. Rheological measurements show a broadening of the gel region, as well as an improvement of the mechanical properties, as assessed by the shear elastic modulus, G' (up to 200% increase). Initial cytocompatibility studies of the nanocomposites show that the materials are non-toxic with viabilities over 70% for NIH3T3 fibroblast cell lines. Overall, the combination of Tetronics and

modified $BaTiO_3$ provides easily customizable systems with promising applications as soft piezoelectric materials.

INTRODUCTION

Nanocomposite hydrogels are emerging as an attractive concept to craft materials with tailored properties, such as mechanical, optical, electronic, as well as promoting a specific biological response (self-healing materials, mechano-actuators, triggered delivery etc).[1] The combination of a polymer gel matrix (which affords mechanical support, phase modulation and a hydrated environment) with nanoparticles (bringing specific functionalities, such as optical, magnetic, piezoelectric, antimicrobial…) is the basis of fascinating properties, resulting from a synergistic interplay between matrix and filler.[1]

A promising type of matrix to produce nanocomposite hydrogels are poloxamines, also known by the commercial name of Tetronics (BASF). They are amphiphilic block copolymers, presenting an original X shape, where each of the four arms is made of a poly(propylene oxide) (PPO) and a poly(ethylene oxide) (PEO) block connected by a central ethylene diamine spacer. The number of PO and EO units that form the arms can be varied, offering a wide range of Mw and HLB values, and hence a rich phase behaviour and custom-made properties, both in terms of thermal and pH response.[2–4] PEO-PPO-based polymeric micelles are now emerging as promising formulation candidates in the biomedical field, being available in large quantities in a large array of architectures, at low-cost, and also showing biological inhibitory activity of drug efflux pumps.[5,6] The more well-known linear counterparts of Tetronics - Pluronic – are currently undergoing clinical trials with the cancer drug doxorubicin[7] and the recent demonstration of the ability of Tetronics to also inhibit ATP-binding cassette transporters in cancer cell lines, responsible for multidrug resistance,[5] added to their pH-responsiveness, has recently brought them into the spotlight as serious contenders in the biomedical field.[6] Indeed, they have been proposed as water-soluble copolymers for injectable formulations,[8] nanocarriers for drug and gene delivery [9,10] and in tissue engineering for bone regeneration.[11]

The introduction of different types of nanoparticles into hydrogels is a successful way to not only improve existing characteristics (such as gel elasticity and toughness), but also add extra functionalities to the hydrogels,[12–14] resulting in new,

functional materials. Extensive research is being carried out in this field covering a wide range of nanofillers, which, used in relatively low amounts, can yield remarkable changes in the final properties. Some examples are clays as natural and synthetic laponites,[15] ceramics as hydroxyapatite (HA) or beta-tricalcium phosphate (β-TCP) for bone regeneration[16,17] and delivery of growth factors.[18] Metallic nanoparticles such as silver and gold constitute other approaches, chosen for their antimicrobial properties,[19] as well as multi-wall carbon nanotubes (MWCNT) and graphene oxide (GO), which are also exploited to create electrically active hydrogels mimicking cardiac tissue with mechano-actuation,[20] and polymer colloids to develop hydrogels for adhesives and surgical sealants.[21]

A substantial amount of work is focusing on inorganic nanoparticles and ceramics as bioactive components in bioengineering,[22,23] such as bioactive silica nanoparticles for improved osteogenesis[24,25] or TiO_2 for antibacterial biodegradable hydrogels.[26] In this work, we focus on Barium Titanate ($BaTiO_3$, BT) nanoparticles, a perovskite-type ferroelectric ceramic that possesses a high dielectric constant with piezoelectric properties (in its tetragonal, orthorhombic and rhombohedral crystalline phases). BT has been replaced in some - mainly electric - applications by multiceramic materials, such as lead zirconate titanates, or PZTs. However, PZTs are not appropriate for biomedical applications due to the high toxicity of the lead component, and BT has been suggested as a good piezoelectric alternative due its better biocompatibility.[27–29] Some examples are as second harmonic generators for imaging applications[30,31] and in drug and gene delivery as nanocarriers and vectors.[27,32] In bone regeneration in particular, BT presents potential as a ceramic filler; its piezoelectricity and interaction with the dipoles formed on the collagen fibres of the inner bone have been shown to promote bone regeneration, as they are able to generate small electrical impulses under minimal mechanic stress, enhancing the cellular and tissue stimulation for the healing process.[33–35]

The main problem to overcome is that ceramic nanoparticles usually present poor processability and high aggregation due to their high area-to-volume ratio.[36,37] This problem may be overcome by surface modification of the nanoparticles. Based on our substantial work on cyclodextrins,[4,38] we explore here the effect of surface modification of BT with cyclodextrins (CDs)[39] prior to their introduction in the hydrogel matrix. Once the nanocomposite hydrogel has been prepared, the physical

and chemical interaction between the matrix and the nanofiller is a determining factor for modulating the properties, which in our case are the changes in the sol-gel transition temperature and the improvement of the mechanical response of the hydrogels.

While it is clear that the introduction of nanoparticles inside a gel matrix may improve the mechanical properties and generally the functionality of the material, there are still few fundamental studies aiming at elucidating structural changes induced by the presence of the nanoparticles, in particular using techniques such as small-angle neutron scattering (SANS). A few exceptions are the studies by Namban and Philip's on the influence of Fe_3O_4 nanoparticles in a matrix of Pluronics,[40] the introduction of clays such as laponite nanoparticles into Pluronic gels[41] and other type of ABA triblock copolymer hydrogels.[42] Annaka et al.[43] reported SANS studies where the introduction of hydrophilized silica nanoparticles (to match the refractive index of the natural lens) impacted the temperature and concentration regime of gel formation; SANS measurements showed that the silica particles did not affect micellar size but decreased their effective volume fraction. Tamborini et al.[44] also used SANS to study the nanocomposite structure of Pluronic crystals and silica nanoparticles as a function of the temperature rate used during preparation, where the volume fraction of the silica nanoparticles is kept low and their size are similar to the micelles.

Within this framework, the objective of this work was to develop soft nanocomposites, using naturally gelling, low-cost poloxamines as a gel matrix, combined with piezoelectric $BaTiO_3$ nanoparticles, chemically modified with cyclodextrins[39] for improved compatibility. The $BatiO_3$ particles are relatively large compared to the micelles and introduced up to high volume fraction (20%). In the first part of this work, we perform a thorough characterisation of the structural changes that lead to T1107 micellization and sol-gel transition, as a function of concentration, pH and temperature, using a combination of techniques (SANS, DLS and FTIR-ATR). Following this, cyclodextrin-modified BT nanoparticles of two different sizes are in the polymer matrix to produce nanocomposite gels, which are characterised both rheologically and spectroscopically, with particular focus on the structural and mechanical changes induced by the addition of the nanofiller. Finally, cytotoxicity and cytocompatibility assays of the nanocomposites at different concentrations, in

solution as well as in the gel phase, are performed, as an initial evaluation of their suitability as biomaterials.

MATERIALS AND METHODS

Materials. Tetronic 1107 (T1107) was a gift from BASF, with a reported composition per arm of 60 EO and 20 PO, HLB 18-23 and average molecular weight 15,000 $g \cdot mol^{-1}$. Inorganic nanoparticles of barium titanate (BT, $BaTiO_3$), with an average diameter of 200 nm were supplied by Nanostructured and Amorphous Materials Inc. (tetragonal crystalline structure, 99.9% purity, ρ = 6.02 $g \cdot cm^{-3}$), while nanoparticles of 50 nm in diameter were supplied by Sigma-Aldrich (cubic crystalline structure, 99.9% purity, ρ = 6.08 $g \cdot cm^{-3}$).

Preparation of $BaTiO_3$ nanoparticles. BT nanoparticles present strong aggregation that leads to rapid precipitation in water. Surface modification of the NPs with β-cyclodextrin (CD) was performed to overcome this problem, according to the two-step procedure described in a previous work,[39] consisting in the generation of hydroxyl groups on the surface by reaction with H_2O_2, followed by mixing with a 10 mM β-CD solution under vigorous stirring. The resulting nanoparticles are centrifuged and washed three times to remove reagents in excess and freeze-dried for storage.

Small-Angle Neutron Scattering (SANS). Small-angle neutron scattering (SANS) experiments were carried out on LOQ instrument at ISIS spallation neutron source (ISIS, Rutherford-Appleton Laboratory, STFC, Didcot, Oxford). LOQ uses incident wavelengths from 2.2 to 10.0 Å, sorted by time-of-flight, with a fixed sample-detector distance of 4.1 m, which provides a range of scattering vectors (q) from 0.009 to 0.29 $Å^{-1}$. The samples were prepared in D_2O (Aldrich, > 99.9% in D) and placed in clean disc-shaped quartz cells (Hellma) of either 1 or 2 mm path length, controlling the temperature from 20 to 50 °C with an external thermostat. In the case of experiments in acidic solutions, the necessary volume of concentrated HCl was added to the samples to reach the desired pH. All scattering data were first normalised for sample transmission and then background-corrected using a quartz cell filled with D_2O to compensate for the inherent instrumental background, and finally corrected for the linearity and efficiency of the detector response using instrument-specific software package. The data were then converted to differential scattering cross-

sections expressed in absolute units of cm^{-1} using the standard procedures at ISIS. Some additional samples (Fig. 6) were measured on D22 at the Institut Laue-Langevin (ILL), The wavelength λ was set at 6 Å, the peak flux of the cold source. The sample-to-detector distance was 4 m with a collimation at 5.6 m and a detector offset of 400 mm to maximize the available q-range using rectangular cells of 1mm of path lenght. All samples for SANS analysis were made in D_2O to ensure sufficient contrast between the polymer and the solvent.

SANS curves were fitted using the SasView 3.1.0 software and a brief explanation of the models can be found in the SI.[45] Scattering curves from T1107 in its unimer form were fitted with a four-arm star-shape polymer model,[46] while micelles were fitted to a core-shell sphere (CSS) model combined with a hard-sphere structure factor. When letting the scattering length density (sld) of the micellar core float, this value converged consistently to values similar to that of pure PO (ρ_{PO} = 3.44×10^{-7} $Å^{-2}$), therefore this parameter was fixed in the fits, reflecting the fact that the micellar core is largely dehydrated, as observed with other poloxamines under dilute conditions.[4,47] Instead, the shell is extensively hydrated, and the level of hydration can be estimated from the fitted value of the sld of the PEO shell, ρ_{shell}. The volume fraction (occupied volume divided by the total volume) of solvent in the corona, x_{solv}, is related to the sld of the shell, PEO block and D_2O by:

$$x_{solv} = \frac{\rho_{shell} - \rho_{EO}}{\rho_{D_2O} - \rho_{EO}} \qquad \text{Eq. 1}$$

The number of water molecules, n_{solv}, in the shell is obtained from:

$$n_{solv} = x_{solv} \frac{v_{shell}}{v_{D_2O}} \qquad \text{Eq. 2}$$

where v_{D_2O} is the volume of a molecule of solvent. The number of water molecules per EO group, n_{solv}/EO, can then be obtained from Eq. 2 and the value of the aggregation number, N_{agg}, is obtained from the hydration of the shell and the structural parameters of the core-shell model. Provided that the amount of water inside the core is negligible, the volume of the micelle is:

$$v_m = N_{agg} v_s + x_{solv} v_{shell} \qquad \text{Eq. 3}$$

where v_s is the volume of a surfactant molecule. N_{agg} can be extracted by introducing into the equation the volume fraction of solvent in the shell, x_{solv}, deduced from Eq. 1.

The nanocomposite data were analysed by a combination of the CSS and a generic power law model (CSS+PL), as well as the combination of different types of paracrystals (SC, BCC and FCC) and the PL model. In all the calculations, the polydispersity of the micelles was taken into account with a value of 0.20 by assuming a Gaussian size distribution.

Dynamic light scattering (DLS). Size distributions of the poloxamine in water were obtained with a photon correlation spectrometer Malvern Zetasizer Nano, with a laser wavelength of 633 nm. The samples were filtered prior to the measurements by 0.22 μm Millex syringe PVDF filters onto semi-micro glass cells, and the temperature of the samples was controlled with 0.1˚C accuracy by the built-in Peltier in the cell compartment. The viscosity and refractive index of the solvent at different temperatures were taken into account to obtain the particle size distribution from the analysis of the autocorrelation function, which was performed with the Zetasizer software in the high resolution mode to better distinguish overlapping distributions.

Infrared spectroscopy. The gelation processes were studied by attenuated total reflectance infrared spectroscopy (FTIR-ATR), using a Nicolette Avatar 360 spectrometer, equipped with a Golden-Gate temperature controlled ATR. The spectra were collected on 0.1 mL samples placed directly on the diamond, at 2 cm^{-1} resolution and 32 scans per spectrum, in the temperature range from 20 to 60 ˚C.

Rheology. Small-amplitude shear oscillatory experiments were performed on a dynamic strain-controlled rheometer ARES (TA Instruments) using plate-plate geometry (25 mm), with a temperature-controlling Peltier unit and a solvent trap. All solutions were left to rest at least one day at room temperature after preparation before conducting the rheological measurements. After loading, a thin layer of low viscosity paraffin oil was added to the geometry edge in order to prevent evaporation. Samples were allowed to rest for a few minutes before the start of the experiments to ensure dissipation of any pre-shearing due to manipulation and loading. Temperature sweeps at constant angular frequency of 6.28 $rad \cdot s^{-1}$ and 1% strain amplitude, within the limit of the linear viscoelastic range as measured by strain amplitude experiments, were conducted at a heating rate of 2 °C/min covering the temperature range from 20 to 80 °C. The gel points are calculated by monitoring the elastic modulus, G', along the temperature sweeps and identifying the gel point as the temperature where there is

a sudden change in slope, corresponding to a sharp increase in G' (corroborated by the calculation of the 2nd derivative).

Preparation of the Nanocomposite Gels. Concentrated solutions of T1107 and NPs were prepared by weighing the required amounts of Tetronic, modified $BaTiO_3$ nanoparticles (50 nm and 200 nm in diameter) and water, D_2O or PBS, followed by mixing. To ensure appropriate dispersion of the NPs in the gel matrix, cycles alternating magnetic stirring, vortex mixing and cooling to 4 ˚C were performed, to facilitate the dissolution of the polymer, while keeping the viscosity low (the viscosity of Poloxamines increases with temperature).

Cytotoxicity Studies. The cytocompatibility of the nanocomposite gels of T1107 and BT was tested on the fibroblast cell line NIH3T3 by means of the tetrazolium assay (MTT), in which the viability of the cells is assessed by the loss of viable cells upon treatment with the compounds of interest. The cells were incubated at 37 ˚C and 5% CO_2 in Dulbecco's modified eagle medium from Life's Technologies, supplemented with 10% fetal bovine serum and 0.1% of penicillin/streptomycin. T1107 solutions were prepared in PBS and filtered through 0.22 μm for sterilization. Cells were seeded into 96-well plates at a concentration of 5×10^4 cells·mL^{-1} and 24 hours later the nanocomposite was introduced into the wells. MTT tests were conducted on day 3 by the addition of MTT 5 mg/mL and incubation for 4 hrs. The formazan absorbance at 540 nm was measured with a Thermo Scientific Multiscan EX microplate reader. DMSO was used as a positive control, and the appropriate negative controls performed by incubating the cells in the absence of the nanocomposite.

RESULTS AND DISCUSION

Self-aggregation of T1107 and phase behaviour: the dilute regime.

The phase diagram of T1107 in water at its natural pH (ca. 7.8) is shown in Fig. 1. At 20% and 40 ˚C, the solution becomes gel-like up to 50 ˚C, with a wider gel region at higher concentrations (spanning 30 ˚C to 80 ˚C at 30%). Gel formation is impeded at acidic pH, due to the protonation of the di-amino middle block. For example, at pH 6, no gel is detected from 25 to 80 ˚C for a 20% mixture. A similar behaviour has been observed with poloxamine T1307, which has a larger molecular weight (18,000 g·mol^{-1}) and higher HLB (> 24); however with this larger poloxamine,

at 20% and pH = 6 a gel phase still exists between 40 and 50 ˚C.[4] More acidic pH totally hinders gel formation. Replacement of H_2O by D_2O slightly shifts the gel phase boundary to higher concentration and temperature (SI, Table 1).

	T (˚C)												
T1107	**20**	**25**	**30**	**35**	**40**	**45**	**50**	**55**	**60**	**65**	**70**	**75**	**80**
5%	○	○	○	○	○	○	○	○	○	○	○	○	○
10%	○	○	○	○	○	○	○	○	○	○	○	○	○
15%	○	○	○	○	○	○	○	○	○	○	○	○	○
20%	□	□	□	□	●	●	●	□	□	□	○	○	○
25%	□	□	□	●	●	●	●	●	●	●	●	●	●
30%	□	●	●	●	●	●	●	●	●	●	●	●	●

Fig. 1. Phase behaviour of T1107 in water. ○ Solution; □ viscous solution; ● gel.

Fig. 2A shows the intensity size distribution of 1% T1107 at different temperatures obtained from DLS measurements. Unimers are detected at 20 ˚C, with a hydrodynamic radius, R_h, of 3.2 nm. Between 30 and 35 ˚C, the distribution broadens and shifts toward higher sizes, reflecting the micellization process. Micelles are fully formed at 40 ˚C, with a R_h nearly constant above that point (7.8 nm). The relative size of the micelles compared to that of the unimers, R_{mic}/R_{unim}, is 2.4, which is intermediate between the larger T1307 (1.6, with N_{EO} = 72, N_{PO} = 23)[2] and the more hydrophobic T904 (2.8, N_{EO} = 15, N_{PO} = 17),[3] suggesting that the micelles of T1107 must contain a relatively low number of unimers, loosely aggregated, as found for T1307 [4] and also reported with Pluronic of high HLB, such as P85.[48] At pH 2.8 (Fig. 2B), the formation of micelles is hindered, resulting in a smaller micellar size of 6.9 nm at 50 ˚C.

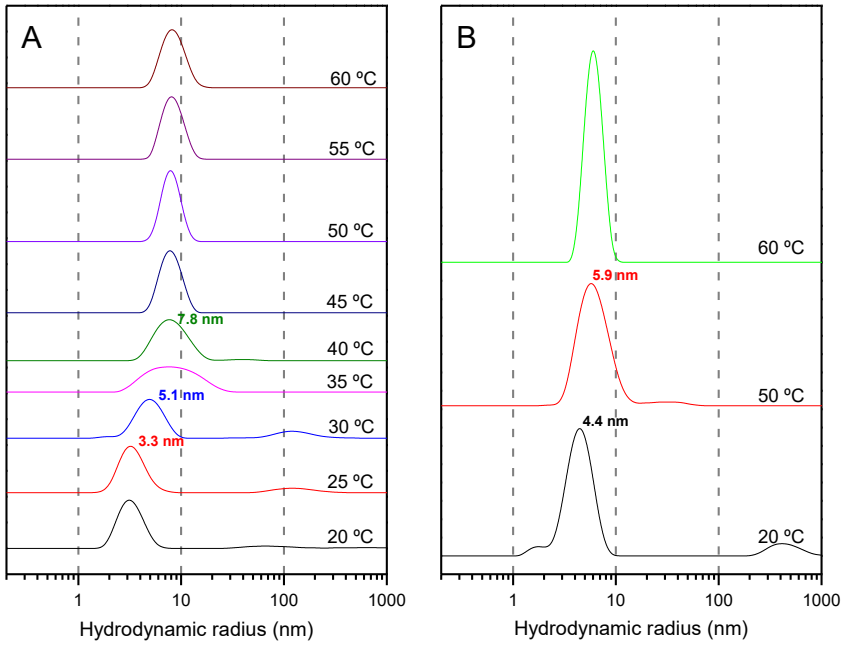

Fig. 2: Intensity size distributions as a function of temperature obtained by DLS for a 1% aqueous solution of T1107 at (A) pH 7.8 and (B) pH 2.8 in H_2O.

More detailed structural information on the unimers and micelles can be obtained from small-angle neutron scattering measurements (SANS); combining these with DLS enables one to unambiguously identify concentration regimes where unimers, micelles, or both are present, thus directing the choice of a suitable fitting model. Fig. 3A shows the scattering curves for a 2% T1107 solution in D_2O. Below 30 ˚C, the poloxamine is in the form of unimers (as established by DLS), whereas at 40 ˚C and 50 ˚C micelles are the dominant species, and the overall scattering increases accordingly. A four-arm star-shape polymer model was shown to successfully describe the unimers.[46] With this model, the radius of gyration, R_g, at 20 ˚C decreases with concentration, from 3.6 nm at 0.5%, to 2.9 nm at 2% and 1.9 nm at 5%; the first value is close to 3.2 nm obtained by DLS for R_h at 1%.

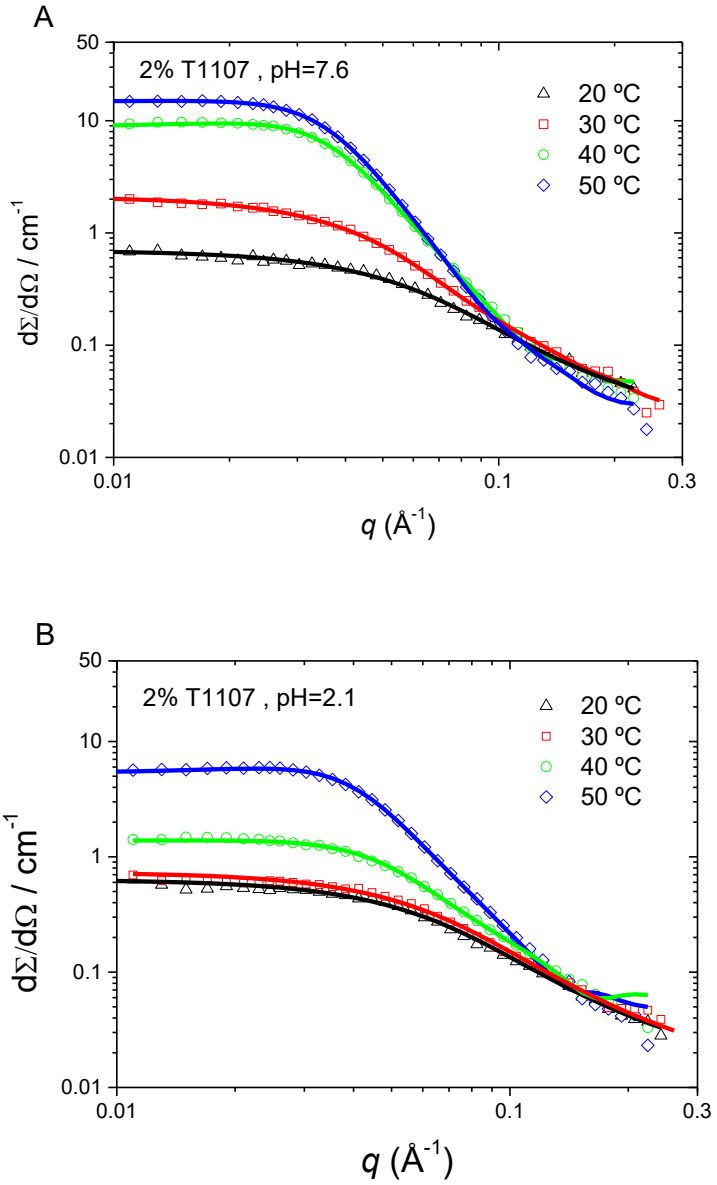

Fig. 3: SANS curves for 2% T1107 solutions in D_2O as a function of temperature at pH 8.1 (A) and pH 2.2 (B). Solid lines are fits to the different models described in the text.

At 40 and 50 ˚C, micelles dominate the scattering, and hence a core-shell sphere model (CSS) combined with a structure factor for hard spheres were used. The fitted and calculated parameters in the dilute regime (2 %) are collected in Table 1 for two values of the pH (data at 0.5% and 5% are provided in SI, Table 2).

Table 1. Micellar parameters of 2% T1107 in D_2O deduced from fits to the SANS data (core-shell model with a hard-sphere structure factor): *Rc* (core radius), *t* (shell thickness), ϕ (volume fraction from the hard-sphere potential), ρ_{shell} (scattering length density of the hydrophilic corona), N_{agg} (aggregation number), nsolv/EO (number of solvent molecules per EO in the shell).

pH	***T / °C***	***R_c / Å***	***t / Å***	***ϕ***	***$\rho_{shell}\times10^6$ /***	***N_{agg}***	***n_{solv}/EO***

					Å^{-2}		
8.1	40	34	47	0.08	5.95	14	20
	50	34	46	0.08	6.06	12	23
2.2	50	30	43	0.08	5.99	9	22

Micellar size is fairly insensitive to temperature or concentration up to 5% (Table 1), with a total radius around 8 nm (in agreement with DLS, Fig. 2A). The sld of the shell, ρ_{shell}, takes values close to D_2O (6.36×10^{-6} Å^{-2}), indicating an extensive solvation of the hydrophilic corona, reflected in the high number of solvent molecules per EO. The aggregation number, N_{agg}, does not vary much with temperature or concentration, while the hydration of the shell (n_{solv}/EO) decreases slightly with concentration, suggesting a more compact micellar structure.

In contrast to temperature and concentration, pH has a strong impact on micellar structure (Fig. 3B, Table 1). At pH 2.2, the low scattering at 20 ˚C and 30 ˚C reflects the presence of unimers with R_g = 2.7 nm (similar to natural pH, at 2.8 nm). At 40 ˚C, both aggregates and micelles coexist (as shown by DLS). At 50 ˚C, the micelles are substantially smaller than at neutral pH (Table 1), in agreement with DLS results (Fig. 2B). N_{agg} is of only 9 molecules per aggregate, comparable to the value of 4 reported in water by static light scattering at pH 2 (37 °C).[2] Thus, a drop in pH can be envisaged as a trigger for the release of a cargo from the interior of the micelles, which do not break fully, thus enabling delivery in a stepwise fashion.

IR spectroscopy can provide information on changes occurring in the chemical surroundings of specific functional groups, such as those occurring in micellization processes or temperature induced sol-gel transitions. There is a precedent of this approach in the literature, where the aggregation of Pluronic F127 [49] and reverse Tetronic 10R5 [3] was followed by monitoring the band at 1085 cm^{-1} (corresponding to the combination of stretching and vibration of the C-O-C from PEO and PPO blocks). The same approach applied to 10% T1107is shown in Figure 4. When increasing the temperature from 20 to 60 ˚C, a shift of the 1085 cm^{-1} band towards higher wavenumbers (blue shift) is observed, as well as a broadening in the bandwidth (FWHM). There is no clear breakpoint in any of the plots, but a smooth change of slope at around 30 ºC (shown with the linear fits) in the maximum of the band, suggesting a small degree of dehydration once micelles form (above the cmc). The

broadening of the IR band also points to the coexistence of different environments or states of dehydration. FTIR-ATR analysis of the T1107 25% is shown on the SI Fig 1. This pattern is qualitatively similar to that obtained for Pluronic F127,[49] although in that previous study the breakpoint was sharper. The more open structure of the T1107 compared to that of the Pluronics may explain that changes in hydration occur in a continuous manner, with less of a sharp change, as the micelles are comparatively less compact, with looser unimers.

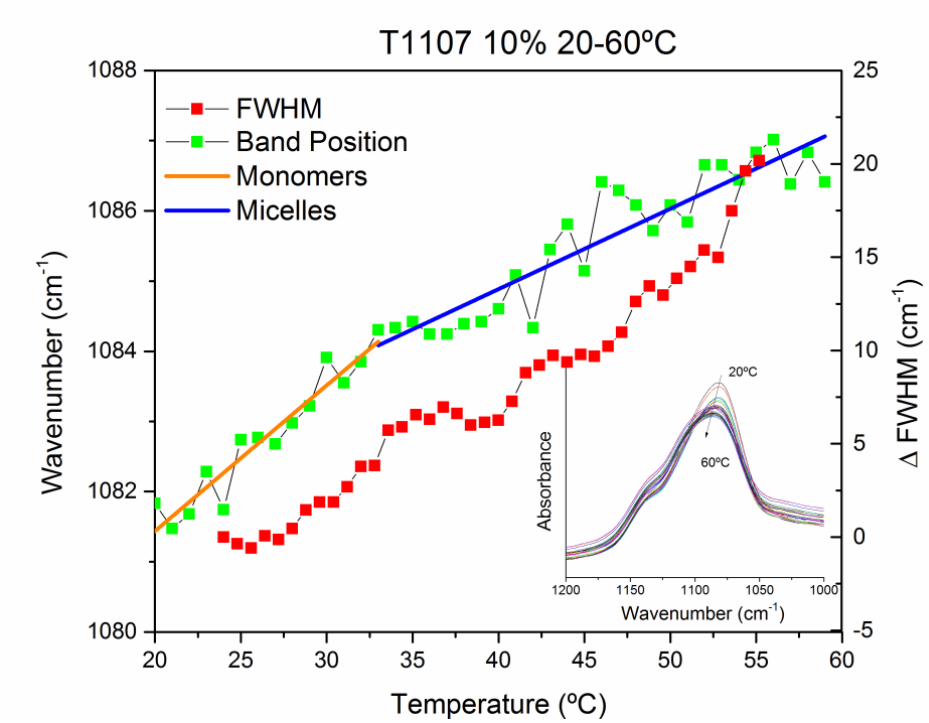

Fig. 4: A FTIR-ATR analysis of the position and FWHM of the 1085 cm^{-1} band of T1107 samples at 10%. The linear fits of the monomer region (orange) and Micelles region (blue) are shown...

The concentrated regime: T1107 gels

Raising the temperature and increasing the concentration of T1107 induces the formation of physical gels (Table 1). Fig. 5A shows the SANS data obtained at 25% T1107 when gradually increasing the temperature from 20 to 50 ˚C; samples turn to gels at 40 ˚C and 50 ˚C (SI, Table 1 for the phase diagram in D_2O). Up to 30 ˚C the solution is viscous and the system consists of a concentrated solution of micelles,

whose interactions are reflected by a strong peak in the mid-*q* range. At 20 ˚C, a fit to thr CSS model reveals micelles of 26 Å core and 33 Å shell (Table 2). Despite the considerably higher concentration, N_{agg} is lower than for 2% micelles at 40 or 50 ˚C, and the shell contains more solvent molecules per EO unit (Table 1), showing that temperature more readily enhances aggregation than concentration. At 30 ˚C, the solution becomes very viscous, producing a high intensity peak around 0.06 $Å^{-1}$ (Fig. 5A), as seen in physical gels consisting of packed micelles.[50] In the gel phase (40 and 50 ˚C), good fits were obtained by using the CSS model with a structure factor for hard spheres, with the sld of the core fixed to that of PO (as for dilute micelles), rather than the paracrystal model used elsewhere for Pluronic gels.[50,51]

Table 2. Micellar parameters of 25% T1107 in D_2O deduced from SANS data analysis. *Rc* (core radius), *t* (shell thickness), ϕ (volume fraction from the hard-sphere potential), ρ_{shell} (scattering length density of the hydrophilic corona), N_{agg} (aggregation number), n_{sol}/EO (number of solvent molecules per EO in the shell).

pH	*T / °C*	*Phase*	R_c / Å	*t* / Å	ϕ	$\rho_{shell} \times 10^6$ / $Å^{-2}$	N_{agg}	n_{sol}/ *EO*
7.6	20	Sol	26	33	0.39	6.29	4	31
	30	Sol-Gel	30	36	0.52	5.98	8	18
	40	Gel	32	36	0.53	5.92	10	16
	50	Gel	33	36	0.53	5.94	10	15
2.1	30	Sol	23	25	0.29	6.05	3	18
	40	Sol	26	27	0.41	5.90	5	14
	50	Sol	28	28	0.44	5.80	7	12

FTIR-ATR data of T1107 gels (Figure 1B SI), unlike what had been observed at 10%, show very little change either in the position of the C-O-C band or its width, suggesting that the chemical environment (i.e., hydration state) of the EO and PO groups remains very similar over the sol-to-gel transition, while it increases more noticeably as a result of micellization (Figure 4A).

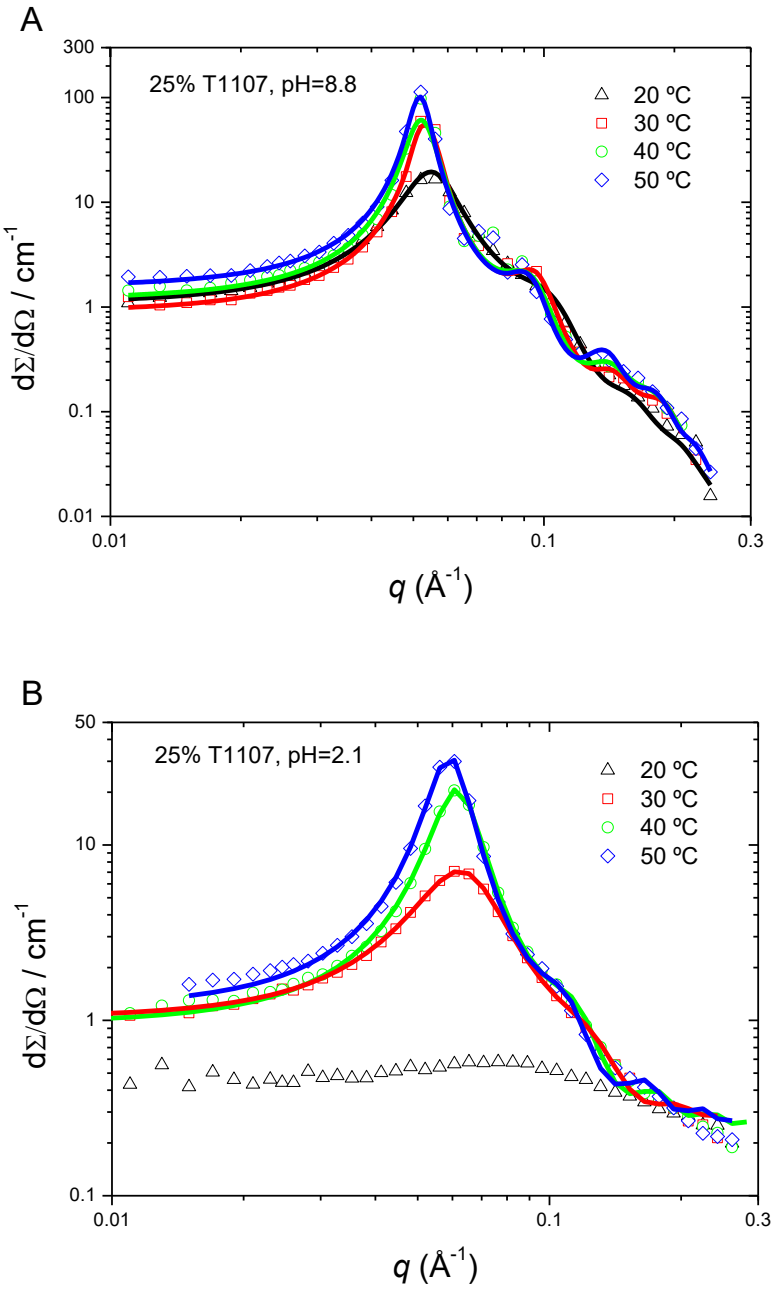

Fig. 5: SANS curves from 25% T1107 solutions in D_2O as a function of temperature at natural pH (A) and at pH 2.1 (B). Solid lines are fits to the models described in the text.

As acidic pH hinders the formation of the micelles, or results in smaller micelles (as observed in the dilute regime), this must have direct consequences on the structure of the gels (Fig. 5B). Clearly, the overall scattering is much lower than at natural pH (Fig. 5A). At 20 ˚C, the lower intensity suggests a transition state, corresponding to a mixture of unimers and micelles, while at higher temperatures (30ºC, 40ºC, 50ºC) the scattering reflects the presence of strongly interacting aggregates, whose structural parameters have been calculated according to a model of CSS with a HS structure

factor. The resulting aggregation numbers are low compared to the gels at natural pH, but the trend with temperature is the same: a dehydration of the shell and increase of N_{agg}, along with an increase in the dimensions of the aggregates. Finally, the volume fractions and sizes are smaller than at natural pH, in agreement with the reduced N_{agg} under acidic conditions.

The volume fraction returned from the fits gives some valuable insights into the structural changes occurring with temperature. At 20 ˚C and natural pH, where the solution is still viscous but no gelation has occurred, a value of 0.39 reflects the concentration of strongly interacting particles. This value increases with temperature and becomes practically constant within the gel region at 0.53. The theoretical volume fraction for a compact packing of spheres fcc is 0.74, 0.68 for a bcc, and 0.52 for a scc arrangement, hence the value obtained would correspond to a simple cubic paracrystal arrangement, as for Pluronic F127.[52] The estimated fraction volume of 0.53, suggests that the arrangement, although displaying some long-range order responsible for the intense diffraction peaks, might rather be a dense mixture of micelles, in close contact, which do not form a completely ordered structure.

In order to test this hypothesis further, a wider range of concentrations of T1107 (10%, 20%, and up to 30%) were measured at 40 ºC, on a different instrument (D22, ILL) and with a set-up that provided a higher resolution of the scattering peaks (Fig. 6). 10% T1107 shows no crystallinity peaks and the scattering curve can be fitted very well with the CSS+HS. The increase in concentration to 20% and 30% leads to a two-fold increase in the intensity and the appearance of sharp scattering peaks in the 0.07-0.09 $Å^{-1}$ range. The higher resolution of this region reveals a peak that was not detectable in the previous set-up (Fig. 5). The CSS+HS model is no longer suitable to describe the data from 20% and above in the higher q region (despite the fit being of higher quality in the lower q region), as it obviates the first peak at 0.07 $Å^{-1}$ (which is best seen in Fig. 7A). As stated above, the presence of these peaks evidence a higher degree of arrangement, probably an intermediate situation between a dense packing of micelles and a paracrystalline structure, which is favoured by the inherent polydispersity of the micelles. BCC fits were proposed for samples with concentrations of 20% T1107 and above, and the diffraction peaks at higher q are better described by this model, giving a sphere radius of 35.1 Å and 35.5 Å for 20%

and 30% solutions and nearest neighbour distance (*dnn*) of 166.8 Å and 155.8 Å, respectively.

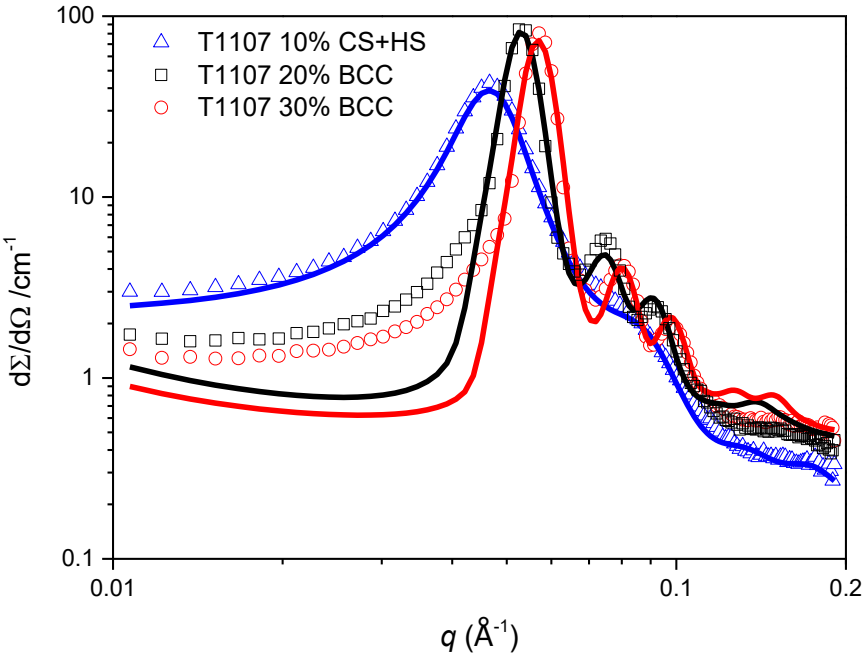

Fig. 6: SANS curves from T1107 10%, 20% and 30% solutions in D_2O at 40 ˚C and natural pH. Solid lines are fits to the models described in the text CSS+HS (10% sample) and BCC (20% and 30% sample). Data measured on D22 (ILL).

Hydrogel nanocomposites

The structure of the nanocomposite gels was studied by SANS with 20% T1107 and a 5% load of $BaTiO_3$ nanoparticles (50 and 200 nm) to achieve a total dry load of 25 %. Figure 7A shows the scattering patterns of the different gel nanocomposites at 40ºC. In addition to the CSS-HS model used for low concentration Tetronic gels, a generic power law was added to account for the scattering of the large inorganic nanoparticles at low *q*.[53,54] The fitted parameters (Table 3) show that the introduction of the nanoparticles in the gel does not seem to affect the size of the micelles, their volume fraction or their aggregation number. As observed for the pure Tetronic gels, the simple CSS+HS model however is not able to not fit the scattering peak adequately in the 0.07-0.09 $Å^{-1}$ *q*-region. These peaks are typical of crystalline or para-crystalline arrangements in the system due to structured nano-domains, as

observed in Pluronic F127 gels [52] and in T1107 gels (Fig. 6). The presence of BT nanoparticles in an already concentrated solution may be able to promote this long-range order arrangement.[55] In order to precisely measure the structural parameters of the nanocomposite gels, the BCC approach was also tested, in combination with a power law model (Figure 7B and Table 4). The introduction of the nanoparticles does not lead to major structural changes in the lattice, namely, a slight tightening of the network with a decrease in the nearest neighbour distance, *dnn* (Table 4), an effect similar to that obtained by increasing the concentration of T1107 (Fig. 6). The values obtained for the T1107+BT nanocomposites fall within the range between the T1107 samples at 20% and 30%. The addition of nanoparticles does not have any notable effect either on the band shift or the FWHM (SI Fig 2). At 25%, T1107 micelles are fully formed at 20 ˚C, and the compaction of the micelles that takes place when increasing the temperature and leads to the sol-gel transition does not involve changes in the local environment that are reflected in the characteristic vibrations of the EO or PO groups.

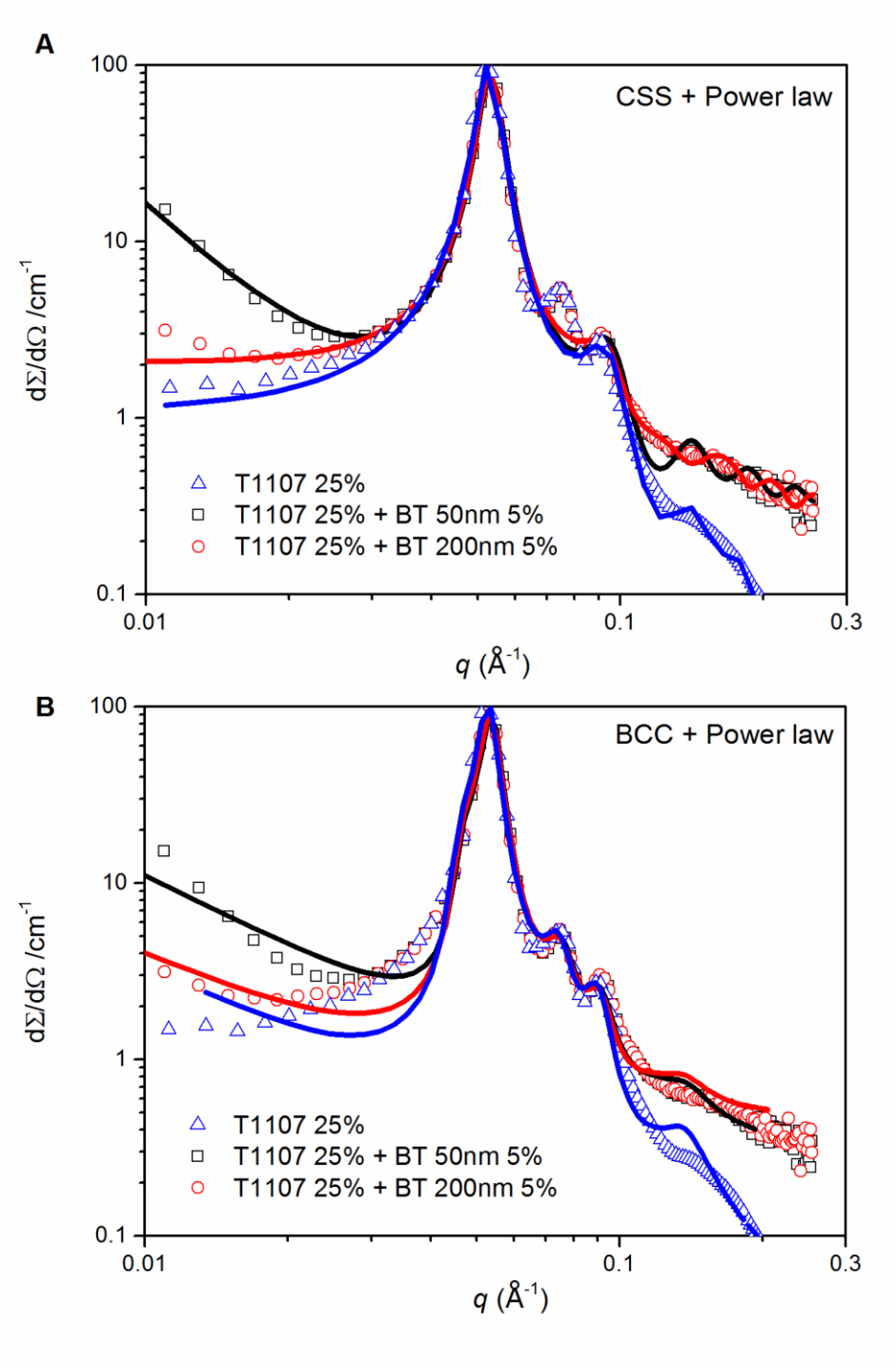

Fig. 7: SANS curves from T1107 25% solutions in D_2O and 20% solutions with 5 wt% of BT 50 nm (black) and BT200 nm (red) at 40 ˚C at natural pH. Solid lines are fits to the models described in the text: CSS+PL (**A**) and BCC+PL (**B**).

Table 3: Micellar parameters of 25% T1107 and 20% T1107 and 5% BT nanoparticles of 50 nm and 200 nm in D_2O extracted from SANS data analysis. R_c (core radius, Å), t (shell thickness, Å), ϕ (volume fraction from the hard-sphere potential), ρ (scattering length density), N_{agg} (aggregation number), n_{solv}/x (number of solvent molecules per EO or PO units in the shell.

Sample	R_c / Å	t / Å	ϕ	$\rho_{shell} \times 10^6$ / Å^{-2}	N_{agg}	n_{sol}/ *EO*
T1107 25%	32	36	0.552	6.13	10	16
T1107 20% BT50 nm	33	34	0.548	6.03	10	16
T1107 20% BT200 nm	32	36	0.554	5.96	10	16

Table 4: Micellar parameters of 25% T1107 and BT nanoparticles of 50 nm and 200 nm in D_2O extracted from SANS data analysis using a BCC model. R_c (core radius, Å), *dnn* (nearest neighbor distance, Å), *D* factor (paracrystal distortion factor)

Sample	R_c / Å	*dnn* / Å	*D factor*
T1107 25%	35	167	0.086
T1107 25% BT50 nm	35	165	0.086
T1107 25% BT200 nm	35	166	0.088

The introduction of nanoparticles in a hydrogel is known to alter its mechanical properties, as well as the thermogelation behaviour of the system .[40,56,57] We thus examine the rheological behaviour of the hydrogel nanocomposites, in particular the

effect of nanoparticle size (50 nm and 200 nm), the relative proportion of poloxamine and NP (varied from 0 to 20% in $BaTiO_3$) and the effect of solvent (both water and phosphate buffered saline, PBS). The introduction of BT nanoparticles is expected to impact gel formation by either affecting the packing of the micelles or increasing connectivity in the network, thus modifying the properties of the system.[1]

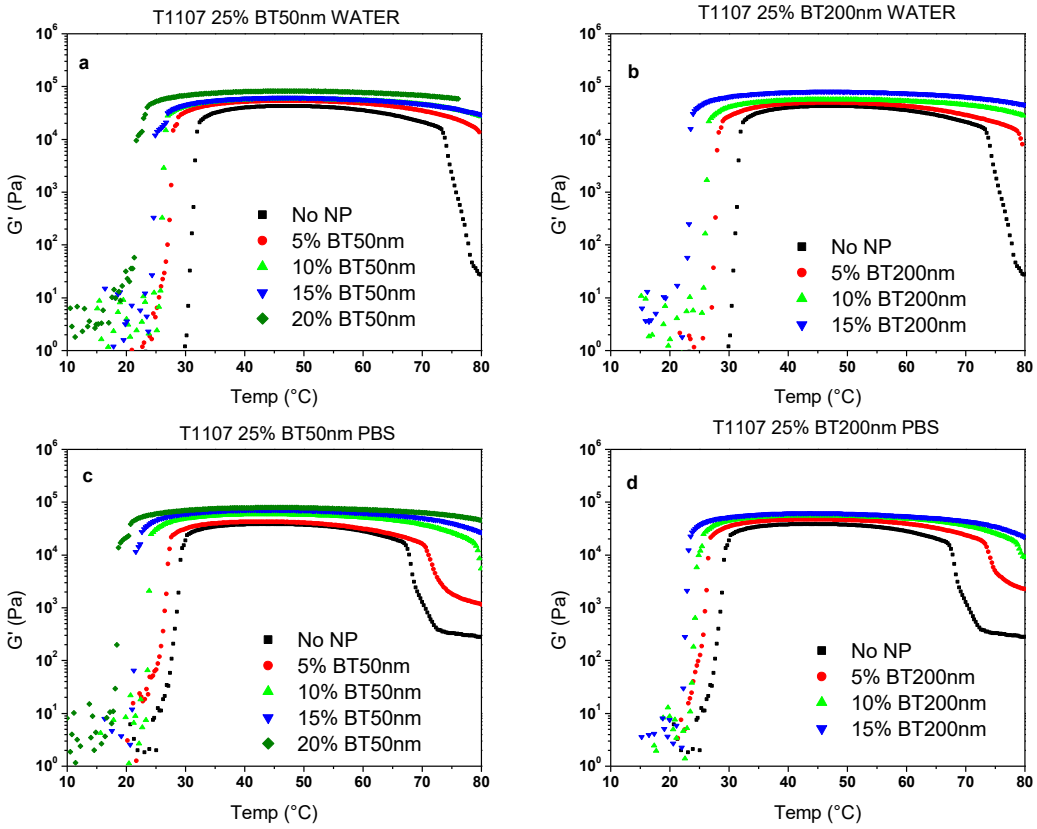

Fig. 8: Temperature sweeps of 25% T1107 with BT nanoparticles of 50nm and 200nm in water and PBS, respectively: **a)** 50 nm BT in water **b)** 200 nm BT in water **c)** 50 nm BT in PBS **d)** 200 nm BT in PBS.

The temperature sweeps showing the elastic modulus between 10 and 80°C (Fig. 8) reveal a broadening of the gel phase region with increasing concentrations of BT from 0% to 20%. The onset of gelation shifts to lower temperatures by as much as 10 ˚C, while the gel-to-sol transition extends beyond 80 ˚C for the highest particle loadings. Replacing water with PBS induces a shift to both sol-gel and gel-sol transitions to lower temperatures (Table 5). This is attributed to the salting out effect caused by PO_4^{3-} anions present in the solvent [58] that reduce the solubility of the PPO blocks, thus lowering the cmc and promoting micellation. At the same time, these anions reduce the capability of the PEO chains to form hydrogen bonds with the

surrounding water, also lowering the cloud point.[59] This overall results in a slightly narrower gel phase, particularly at 0% and 5% BT, but at higher BT loading (above 10%), the effect of PBS is compensated by the effect of the filler, resulting in a gel phase extending beyond 80 ˚C.

Table 5: Rheological Data for T1107 25% with 50 nm (BT50) and 200 nm (BT200) $BaTiO_3$ nanoparticles.

Sample	Solvent	Gel Formation Temperature (˚C)	Span of the gel phase (˚C)	G' Max (KPa)	Tan (δ)
T1107 25%	Water	32	41	42.6	0.081
	PBS	29	38	38.3	0.057
5% BT50	Water	28	51	53.7	0.046
	PBS	27	43	42.6	0.048
10% BT50	Water	27	53	59.1	0.020
	PBS	24	55	59.3	0.021
15% BT50	Water	25	53	62.2	0.011
	PBS	22	57	72.4	0.020
20% BT50	Water	23	57	83.1	0.016
	PBS	18	60	80.2	0.021
5% BT200	Water	28	50	49.4	0.028
	PBS	27	46	47.0	0.049
10% BT200	Water	26	53	57.4	0.022
	PBS	24	52	56.6	0.031
15% BT200	Water	23	56	81.2	0.014
	PBS	23	57	63.1	0.017

An important effect of the addition of the nanoparticles, beyond extending the gel phase, is the increase in the elastic modulus (Table 5, Fig. 9). A direct relationship is observed between the amount of nanoparticles and the increase in G', with, however, no effect of particle sizes up to 10% concentration.

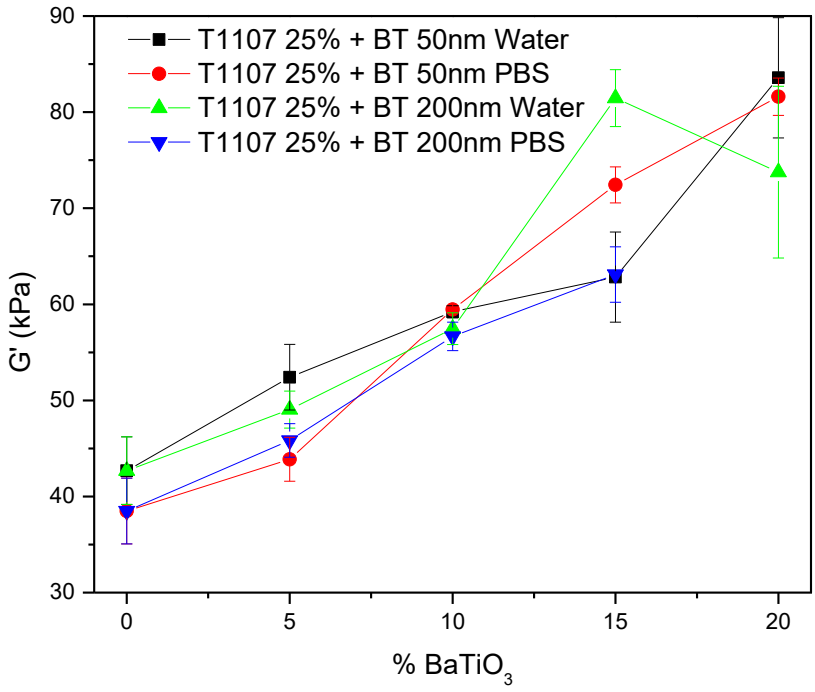

Figure 9. Change in elastic modulus (G') as a function of BT concentration in T1107 25% samples.

There is, however, quite some variation between repeats at high particle loading (20%) and this erratic behaviour may be attributed due to the difficulty in achieving sample homogeneity, effect also seen by Tamborini et al in their work in micellar polycristals.[44] The overall increase in G' and sharp decrease in tan (δ) (Table 5) suggests that the introduction of the cyclodextrin-coated nanoparticles leads to a more rigid and connected network. Comparing tan (δ) values at the same compositions for the two different solvents shows again that the presence of charges from PBS leads to an increase in the liquid-like behaviour of the system and a looser packing of the network.

Cytotoxicity studies.

Previous investigations have reported good cytotoxicity results for BT alone.[30,60,61] The surface modified BT with CDs, which helps to stabilize the nanoparticles in solution, display excellent viability of the cells, even up to concentrations of 200 μg/mL.[39] Figure 10 shows the MTT results for the T1107 hydrogels at different concentrations with and without BT200-βCD nanoparticles.

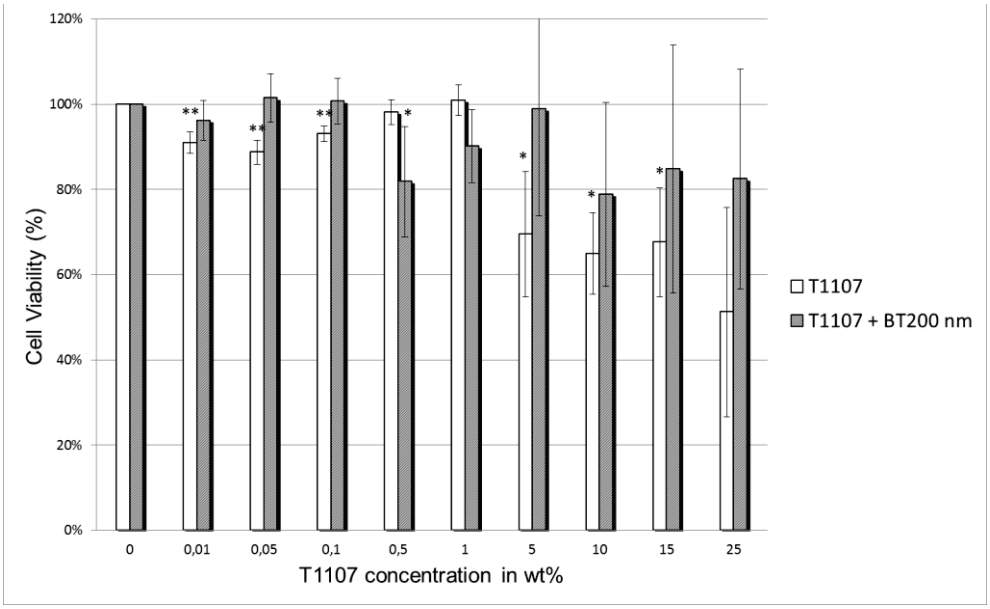

Fig. 10: MTT results for NIH3T3 cells and T1107 (White bars) and T1107 with BT 200 nm nanoparticles modified with β-CD (Black bars). * denotes $p<0.05$ and ** denotes $p<0.01$ by ANOVA variance and Student's T tests.

Tetronic T1107 shows cytotoxicity scores of 0 (<90%) and 1 (70-90%) after 72h at all the concentrations but the highest one (25 wt%), with and without BT nanoparticles. With poloxamine concentration above 1 wt%, it is difficult to achieve reproducible results in fibroblast cell lines (large standard deviations are shown as error bars), which is in accordance with some results reported in the literature.[11] Fibroblasts are known to be particularly sensitive to nutritional requirements compared to other cell lines.[62] This may be combined with the fact that at higher concentrations (>1% T1107) and 37.5 ºC, the high density of micelles or gel may prevent the nutrients to have continuous access to the cell layer in the 96-well plate, and thus contribute to the high deviations. The introduction of the CD-coated nanoparticles generally improves the viability of the cells, results that are in line with what has been reported for BT nanoparticles alone. Altogether, the introduction of BT in the hydrogel and the formation of the nanocomposites do not produce an increase in the toxic effect in the studied cells, thus showing promise for these nanocomposite gels as biomedical materials.

Conclusions

The phase behaviour of the hydrophilic, X-shaped poloxamine Tetronic T1107 has been fully characterised, using a combination of DLS and SANS. At low concentrations and above 30˚C, the amphiphile forms spherical micelles with a dehydrated core and a highly hydrated shell, with aggregation numbers relatively small, mostly due to the hydrophilicity of the polymer, with dimensions that do not depend much on the temperature or concentration. Micellar size is notably affected by the degree of protonation of the central amine spacer, forming loose hydrated aggregates. In the high-concentration regime, T1107 forms gels. SANS data analysis shows that upon gelation the micelles become dehydrated, and long-range order is detected through the appearance of sharp scattering peaks, revealing a BCC order. The presence of BT nanoparticles modified with CDs produces substantial changes in the rheological behaviour of the system. By adjusting the concentration of the nanoparticles, the sol-gel transition temperature of 25% T1107 can be tailored, with a maximum reduction in the gelation temperature of 12 ºC, as well as an increase of the same magnitude in the gel-sol transition, thus leading to a broadening of the gel phase region. At the same time, the elastic modulus G' of the nanocomposite increases up to 200% by incorporating the BT nanoparticles, and follows a linear trend with the concentration of the nanofiller. Thus, in addition to their inherent piezoelectric properties, the nanoparticles provide a handle to tune gelation point and elastic gel modulus, which is of interest for the preparation of injectable (thermoresponsive) hydrogels. From the structural point of view, the presence of the modified BT nanoparticles do not disturb the BCC arrangement of the micelles in the gels. Overall, the effect of filler size (50 nm vs 200 nm) is largely negligible, both on the macroscopic scale (rheology) and the nanostructure. Acidic conditions inhibit the formation of a gel phase, leaving a concentrated solution of small aggregates formed by extensively hydrated oligomers. The cytotoxicity of the nanocomposites was assessed both at high and low concentrations. Viability of fibroblasts at low concentration of poloxamine (up to 1 wt%), show excellent results (above 90% viability) for both the T1107 and the nanocomposite. At higher concentrations (1 wt% to 25 wt% T1107 with and without BT) the viability levels are between 70-90%, presenting higher variability for that specific cell line due to the presence of the micelles interfering with the nutrition demands of the cells. Overall, these results are promising for the further development of these composite materials for biomedical applications.

Acknowledgements

The authors thank ISIS and ILL for the provision of beam time and R. Heenan (Rutherford Appleton Laboratory), Isabelle Grillo and E. Larrañeta (Queen's University Belfast) for his assistance with the SANS experiments. Prof. G. Martínez de Tejada is acknowledged for his invaluable assistance with the cell viability studies. Financial support from projects MAT2014-59116-C2-2-R of the Spanish MINECO is acknowledged. G.G.-G. is grateful to the Vicerrectorado de Relaciones Internacionales of the UN for the mobility grant for his sabbatical leave at KCL and Asociación de Amigos of the University of Navarra for the PhD grant of R. Serra-Gómez.

Supporting information

General description on the different models for fitting the SANS data. Phase diagram of T1107 in D_2O. Fitting results for T1107 0.5 and 5% (CSS-HS). FTIR analysis of T1107 and nanocomposites with $BaTiO_3$.

References

(1) da Silva, M. A.; Dreiss, C. A. Soft Nanocomposites: Nanoparticles to Tune Gel Properties. *Polym. Int.* **2016**, *65*, 268–279.
(2) Gonzalez-Lopez, J.; Alvarez-Lorenzo, C.; Taboada, P.; Sosnik, A.; Sandez-Macho, I.; Concheiro, A. Self-Associative Behavior and Drug-Solubilizing Ability of Poloxamine (Tetronic) Block Copolymers. *Langmuir* **2008**, *24*, 10688–10697.
(3) Larrañeta, E.; Isasi, J. R. Phase Behavior of Reverse Poloxamers and Poloxamines in Water. *Langmuir* **2013**.
(4) González-Gaitano, G.; da Silva, M. a.; Radulescu, A.; Dreiss, C. a. Selective Tuning of the Self-Assembly and Gelation of a Hydrophilic Poloxamine by Cyclodextrins. *Langmuir* **2015**, *31*, 5645–5655.
(5) Cuestas, M. L.; Sosnik, A.; Mathet, V. L. Poloxamines Display a Multiple Inhibitory Activity of ATP-Binding Cassette (ABC) Transporters in Cancer Cell Lines. *Mol. Pharm.* **2011**, *8*, 1152–1164.
(6) Alvarez-Lorenzo, C.; Sosnik, A.; Concheiro, A. PEO-PPO Block Copolymers for Passive Micellar Targeting and Overcoming Multidrug Resistance in Cancer Therapy. *Curr. Drug Targets* **2011**, *12*, 1112–1130.
(7) Alakhova, D. Y.; Kabanov, A. V. Pluronics and MDR Reversal: An Update. *Mol. Pharm.* **2014**, *11*, 2566–2578.
(8) Annaka, M.; Mortensen, K.; Vigild, M. E.; Matsuura, T.; Tsuji, S.; Ueda, T.;

Tsujinaka, H. Design of an Injectable in Situ Gelation Biomaterials for Vitreous Substitute. *Biomacromolecules* **2011**, *12*, 4011–4021.
(9) Carmen Alvarez-Lorenzo, Ana Rey-Rico, Alejandro Sosnik, Pablo Taboada, A. C. Poloxamine-Based Nanomaterials for Drug Delivery. *Front. Biosci.* **2010**, *2*, 424–440.
(10) Zhang, J.; Sen, A.; Cho, E.; Lee, J. S.; Webb, K. Poloxamine/fibrin Hybrid Hydrogels for Non-Viral Gene Delivery. *J. Tissue Eng. Regen. Med.* **2014**.
(11) Rey-Rico, A.; Silva, M.; Couceiro, J.; Concheiro, A.; Alvarez-Lorenzo, C. Osteogenic Efficiency of in Situ Gelling Poloxamine Systems with and without Bone Morphogenetic Protein-2. *Eur. Cells Mater.* **2011**, *21*, 317–340.
(12) Balazs, A. C.; Emrick, T.; Russell, T. P. Nanoparticle Polymer Composites : Meet Two Small Worlds. *Science (80-.).* **2013**, *314*, 1107–1110.
(13) Schexnailder, P.; Schmidt, G. Nanocomposite Polymer Hydrogels. *Colloid Polym. Sci.* **2008**, *287*, 1–11.
(14) Chu, Z.; Dreiss, C. a; Feng, Y. Smart Wormlike Micelles. *Chem. Soc. Rev.* **2013**, *42*, 7174–7203.
(15) Wu, C.-J.; Gaharwar, A. K.; Chan, B. K.; Schmidt, G. Mechanically Tough Pluronic F127/Laponite Nanocomposite Hydrogels from Covalently and Physically Cross-Linked Networks. *Macromolecules* **2011**, *44*, 8215–8224.
(16) Gaharwar, A. K.; Dammu, S. a; Canter, J. M.; Wu, C.-J.; Schmidt, G. Highly Extensible, Tough, and Elastomeric Nanocomposite Hydrogels from Poly(ethylene Glycol) and Hydroxyapatite Nanoparticles. *Biomacromolecules* **2011**, *12*, 1641–1650.
(17) Chen, Q.; Zhu, C.; Thouas, G. A. Progress and Challenges in Biomaterials Used for Bone Tissue Engineering: Bioactive Glasses and Elastomeric Composites. *Prog. Biomater.* **2012**, *1*, 2.
(18) Nguyen, L. H.; Annabi, N.; Nikkhah, M.; Bae, H.; Binan, L.; Park, S.; Kang, Y.; Yang, Y.; Khademhosseini, A. Vascularized Bone Tissue Engineering: Approaches for Potential Improvement. *Tissue Engineering Part B: Reviews*, 2012, *18*, 363–382.
(19) Fan, Z.; Liu, B.; Wang, J.; Zhang, S.; Lin, Q.; Gong, P.; Ma, L.; Yang, S. A Novel Wound Dressing Based on Ag/Graphene Polymer Hydrogel: Effectively Kill Bacteria and Accelerate Wound Healing. *Adv. Funct. Mater.* **2014**, *24*, 3933–3943.
(20) Shin, S. R.; Aghaei-Ghareh-Bolagh, B.; Dang, T. T.; Topkaya, S. N.; Gao, X.; Yang, S. Y.; Jung, S. M.; Oh, J. H.; Dokmeci, M. R.; Tang, X.; et al. Cell-Laden Microengineered and Mechanically Tunable Hybrid Hydrogels of Gelatin and Graphene Oxide. *Adv. Mater.* **2013**, *25*, 6385–6391.
(21) Cho, E.; Lee, J. S.; Webb, K. Formulation and Characterization of Poloxamine-Based Hydrogels as Tissue Sealants. *Acta Biomater.* **2012**, *8*, 2223–2232.
(22) Wang, H.; Bongio, M.; Farbod, K.; Nijhuis, A. W. G.; Van Den Beucken, J.; Boerman, O. C.; Van Hest, J. C. M.; Li, Y.; Jansen, J. A.; Leeuwenburgh, S. C. G. Development of Injectable Organic/inorganic Colloidal Composite Gels Made of Self-Assembling Gelatin Nanospheres and Calcium Phosphate Nanocrystals. *Acta Biomater.* **2014**, *10*, 508–519.
(23) Pina, S.; Oliveira, J. M.; Reis, R. L. Natural-Based Nanocomposites for Bone Tissue Engineering and Regenerative Medicine: A Review. *Adv. Mater.* **2015**, 1143–1169.
(24) Schiraldi, C.; D'Agostino, A.; Oliva, A.; Flamma, F.; De Rosa, A.; Apicella, A.; Aversa, R.; De Rosa, M. Development of Hybrid Materials Based on

Hydroxyethylmethacrylate as Supports for Improving Cell Adhesion and Proliferation. *Biomaterials* **2004**, *25*, 3645–3653.
(25) Gaharwar, A. K.; Mihaila, S. M.; Swami, A.; Patel, A.; Sant, S.; Reis, R. L.; Marques, A. P.; Gomes, M. E.; Khademhosseini, A. Bioactive Silicate Nanoplatelets for Osteogenic Differentiation of Human Mesenchymal Stem Cells. *Adv. Mater.* **2013**, *25*, 3329–3336.
(26) Si, S.; Zhou, R.; Xing, Z.; Xu, H.; Cai, Y.; Zhang, Q. A Study of Hybrid Organic/inorganic Hydrogel Films Based on in Situ-Generated TiO2 Nanoparticles and Methacrylated Gelatin. *Fibers Polym.* **2013**, *14*, 982–989.
(27) Jeong, C. K.; Kim, I.; Park, K.-I.; Oh, M. H.; Paik, H.; Hwang, G.-T.; No, K.; Nam, Y. S.; Lee, K. J. Virus-Directed Design of a Flexible BaTiO3 Nanogenerator. *ACS Nano* **2013**, *7*, 11016–11025.
(28) Sakai, T.; Hoshiai, S.; Nakamachi, E. Biochemical Compatibility of PZT Piezoelectric Ceramics Covered with Titanium Thin Film. *J. Optoelectron. Adv. Mater.* **2006**, *8*, 1435–1437.
(29) Tsuchiya, K.; Akagawa, Y.; Uetsuji, Y.; Nakamachi, E. Design of Biocompatible High-Piezoelectric BaTiO3 with Additives. In *Smart Nano-Micro Materials and Devices*; Juodkazis, S., Gu, M., Eds.; International Society for Optics and Photonics, 2011; p 82042A.
(30) Dempsey, C.; Lee, I.; Cowan, K. R.; Suh, J. Coating Barium Titanate Nanoparticles with Polyethylenimine Improves Cellular Uptake and Allows for Coupled Imaging and Gene Delivery. *Colloids Surf. B. Biointerfaces* **2013**, *112*, 108–112.
(31) Hsieh, C.-L.; Grange, R.; Pu, Y.; Psaltis, D. Bioconjugation of Barium Titanate Nanocrystals with Immunoglobulin G Antibody for Second Harmonic Radiation Imaging Probes. *Biomaterials* **2010**, *31*, 2272–2277.
(32) Ciofani, G.; Danti, S.; Moscato, S.; Albertazzi, L.; D'Alessandro, D.; Dinucci, D.; Chiellini, F.; Petrini, M.; Menciassi, a. Preparation of Stable Dispersion of Barium Titanate Nanoparticles: Potential Applications in Biomedicine. *Colloids Surf. B. Biointerfaces* **2010**, *76*, 535–543.
(33) Barrère, F.; Mahmood, T. a.; de Groot, K.; van Blitterswijk, C. a. Advanced Biomaterials for Skeletal Tissue Regeneration: Instructive and Smart Functions. *Mater. Sci. Eng. R Reports* **2008**, *59*, 38–71.
(34) Feng, J.; Yuan, H.; Zhang, X. Promotion of Osteogenesis by a Piezoelectric Biological Ceramic. *Biomaterials* **1997**, *18*, 1531–1534.
(35) Baxter, F. R.; Turner, I. G.; Bowen, C. R.; Gittings, J. P.; Chaudhuri, J. B. An in Vitro Study of Electrically Active Hydroxyapatite-Barium Titanate Ceramics Using Saos-2 Cells. *J. Mater. Sci. Mater. Med.* **2009**, *20*, 1697–1708.
(36) Blanco-Lopez, M. C.; Rand, B.; Riley, F. L. The Properties of Aqueous Phase Suspensions of Barium Titanate. *J. Eur. Ceram. Soc.* **1997**, *17*, 281–287.
(37) Paik, U.; Yeo, J.-G.; Lee, M.-H.; Hackley, V. A.; Jung, Y.-G. Dissolution and Reprecipitation of Barium at the Particulate BaTiO3–aqueous Solution Interface. *Mater. Res. Bull.* **2002**, *37*, 1623–1631.
(38) Serra-Gómez, R.; Tardajos, G.; González-Benito, J.; González-Gaitano, G. Rhodamine Solid Complexes as Fluorescence Probes to Monitor the Dispersion of Cyclodextrins in Polymeric Nanocomposites. *Dye. Pigment.* **2012**, *94*, 427–436.
(39) Serra-Gómez, R.; Martinez-Tarifa, J. M.; González-Benito, J.; González-Gaitano, G. Cyclodextrin-Grafted Barium Titanate Nanoparticles for Improved Dispersion and Stabilization in Water-Based Systems. *J. Nanoparticle Res.*

2016, *18*, 24.
(40) Nambam, J. S.; Philip, J. Thermogelling Properties of Triblock Copolymers in the Presence of Hydrophilic Fe3O4 Nanoparticles and Surfactants. *Langmuir* **2012**, *28*, 12044–12053.
(41) Sun, K.; Raghavan, S. R. Thermogelling Aqueous Fluids Containing Low Concentrations of Pluronic F127 and Laponite Nanoparticles. *Langmuir* **2010**, *26*, 8015–8020.
(42) Agrawal, S. K.; Sanabria-Delong, N.; Tew, G. N.; Bhatia, S. R. Nanoparticle-Reinforced Associative Network Hydrogels. *Langmuir* **2008**, *24*, 13148–13154.
(43) Annaka, M.; Mortensen, K.; Matsuura, T.; Ito, M.; Nochioka, K.; Ogata, N. Organic–inorganic Nanocomposite Gels as an in Situ Gelation Biomaterial for Injectable Accommodative Intraocular Lens. *Soft Matter* **2012**, *8*, 7185.
(44) Tamborini, E.; Ghofraniha, N.; Oberdisse, J.; Cipelletti, L.; Ramos, L. Structure of Nanoparticles Embedded in Micellar Polycrystals. *Langmuir* **2012**, *28*, 8562–8570.
(45) Http://www.sasview.org/, Developed by the DANSE Project under NSF Award DMR-0520547.
(46) Benoit, H. On the Effect of Branching and Polydispersity on the Angular Distribution of the Light Scattered by Gaussian Coils. *J. Polym. Sci.* **1953**, *11*, 507–510.
(47) González-Gaitano, G.; Müller, C.; Radulescu, A.; Dreiss, C. A. Modulating the Self-Assembly of Amphiphilic X-Shaped Block Copolymers with Cyclodextrins: Structure and Mechanisms. *Langmuir* **2015**, *31*, 4096–4105.
(48) Kabanov, A. V.; Batrakova, E. V.; Alakhov, V. Y. Pluronic® Block Copolymers as Novel Polymer Therapeutics for Drug and Gene Delivery. *J. Control. Release* **2002**, *82*, 189–212.
(49) Su, Y. L.; Wang, J.; Liu, H. Z. FTIR Spectroscopic Investigation of Effects of Temperature and Concentration on PEO-PPO-PEO Block Copolymer Properties in Aqueous Solutions. *Macromolecules* **2002**, *35*, 6426–6431.
(50) Okabe, S.; Sugihara, S.; Aoshima, S.; Shibayama, M. Heat-Induced Self-Assembling of Thermosensitive Block Copolymer. Rheology and Dynamic Light Scattering Study. *Macromolecules* **2003**, *36*, 4099–4106.
(51) Dreiss, C. A.; Nwabunwanne, E.; Liu, R.; Brooks, N. J. Assembling and de-Assembling Micelles: Competitive Interactions of Cyclodextrins and Drugs with Pluronics. *Soft Matter* **2009**, *5*, 1888.
(52) Dreiss, C. A.; Nwabunwanne, E.; Liu, R.; Brooks, N. J. Assembling and de-Assembling Micelles : Competitive Interactions of Cyclodextrins and Drugs with Pluronics †. *Soft Matter* **2009**, *5*, 1888–1896.
(53) Campanella, A.; Di, Z.; Luchini, A.; Paduano, L.; Klapper, A.; Herlitschke, M.; Petracic, O.; Appavou, M. S.; Müller-Buschbaum, P.; Frielinghaus, H.; et al. Nanocomposites Composed of HEUR Polymer and Magnetite Iron Oxide Nanoparticles: Structure and Magnetic Response of the Hydrogel and Dried State. *Polymer (Guildf).* **2015**, *60*, 176–185.
(54) Kanapathipillai, M.; Yusufoglu, Y.; Rawal, a.; Hu, Y.-Y.; Lo, C.-T.; Thiyagarajan, P.; Kalay, Y. E.; Akinc, M.; Mallapragada, S.; Schmidt-Rohr, K. Synthesis and Characterization of Ionic Block Copolymer Templated Calcium Phosphate Nanocomposites. *Chem. Mater.* **2008**, *20*, 5922–5932.
(55) Mortensen, K. Structural Study on the Micelle Formation of PEO-PPO-PEO Triblock Copolymer in Aqueous Solutions. *Macromolecules* **1993**, *26*, 805–812.

(56) Shen, J.; Xu, G.; Xin, X.; Wang, L.; Song, Z.; Zhang, H.; Tong, L.; Yang, Z. Supramolecular Hydrogels of α-Cyclodextrin/reverse Poloxamines/carbon-Based Nanomaterials and Its Multi-Functional Application. *RSC Adv.* **2015**, *5*, 40173–40182.
(57) Cha, C.; Shin, S. R.; Gao, X.; Annabi, N.; Dokmeci, M. R.; Tang, X. S.; Khademhosseini, A. Controlling Mechanical Properties of Cell-Laden Hydrogels by Covalent Incorporation of Graphene Oxide. *Small* **2014**, *10*, 514–523.
(58) Pandit, N.; Trygstad, T.; Croy, S.; Bohorquez, M.; Koch, C. Effect of Salts on the Micellization, Clouding, and Solubilization Behavior of Pluronic F127 Solutions. *J. Colloid Interface Sci.* **2000**, *222*, 213–220.
(59) Wang, Y.; Shi, X.; Ren, L.; Yao, Y.; Zhang, F.; Wang, D.-A. Poly(lactide-Co-Glycolide)/titania Composite Microsphere-Sintered Scaffolds for Bone Tissue Engineering Applications. *J. Biomed. Mater. Res. B. Appl. Biomater.* **2010**, *93*, 84–92.
(60) Ciofani, G.; Danti, S.; D'Alessandro, D.; Moscato, S.; Petrini, M.; Menciassi, A. Barium Titanate Nanoparticles: Highly Cytocompatible Dispersions in Glycol-Chitosan and Doxorubicin Complexes for Cancer Therapy. *Nanoscale Res. Lett.* **2010**, *5*, 1093–1101.
(61) FarrokhTakin, E.; Ciofani, G.; Gemmi, M.; Piazza, V.; Mazzolai, B.; Mattoli, V. Synthesis and Characterization of New Barium Titanate Core–gold Shell Nanoparticles. *Colloids Surfaces A Physicochem. Eng. Asp.* **2012**, *415*, 247–254.
(62) Park, J.-C.; Park, B. J.; Lee, D. H.; Suh, H.; Kim, D.-G.; Kwon, O.-H. Evaluation of the Cytotoxicity of Polyetherurethane (PU) Film Containing Zinc Diethyldithiocarbamate (ZDEC) on Various Cell Lines. *Yonsei Med. J.* **2002**, *43*, 518–526.

TOC GRAPHIC

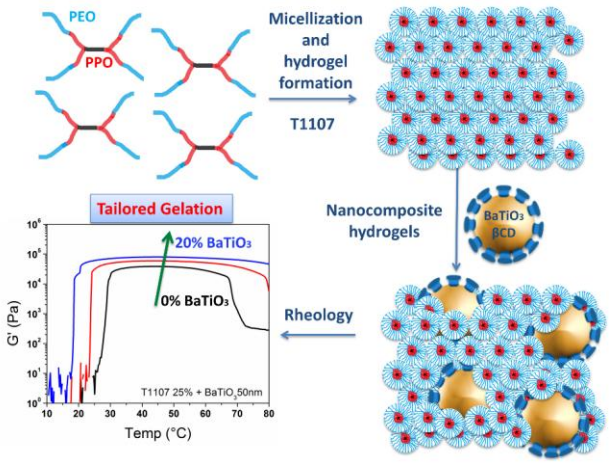
PEO
PPO
Micellization and hydrogel formation
T1107
Nanocomposite hydrogels
BaTiO3 βCD
Rheology
Tailored Gelation
20% BaTiO3
0% BaTiO3
T1107 25% + BaTiO3 50nm
G' (Pa)
Temp (°C)